

High Resolution Imaging Microscope (HIRIM)

Mary M. Yang, William J. Coleman, Chris M. Silva, Michael R. Dilworth,
Edward J. Bylina, and Douglas C. Youvan *

*Corresponding Author:

KAIROS Scientific Inc.
Bldg. 62
3350 Scott Blvd.
Santa Clara, CA 95054 USA

E-mail: dyouvan@kairos-scientific.com

Website: www.kairos-scientific.com

Received: 11/15/97

Accepted: 1/28/98

Research Editor: Dr. Simon Delagrave

Abstract

The High Resolution Imaging Microscope (HIRIM) is a microspectrophotometer which is capable of determining the individual absorption spectra of complex groupings of microscopic features in a massively parallel manner. We demonstrate here the feasibility of obtaining high resolution spectra of pigmented or stained biological material with this instrument. The spectra of individual marine and freshwater microorganisms and hematoxylin and eosin stained thin sections for histopathology are presented as examples of HIRIM's ability to extract spectral data from morphological features. To perform this task, a digital imaging spectrophotometer (DIS) previously configured for macroscopic samples has been redesigned and constructed. The prototype HIRIM instrument is able to simultaneously acquire spatial and spectral information on hundreds of algae and cyanobacteria immobilized on slides. Absorption due to chlorophyll, phycobilins, carotenoids and other pigments can be readily determined from individual cell spectra. The utility of this microscope for potential applications in microbiology, medicine, remote sensing, biotechnology, engineering, materials processing and quality control are discussed.

Introduction

Sample types. The use of dyes and pigments to aid in identifying salient features of optically transparent materials is of paramount importance to many types of microscopic analyses. In some cases, the sample under analysis has been colored by endogenous biosynthetic chromophores (as in photosynthetic organisms) or by dyes incorporated into the material during a manufacturing process (as in certain organic thin films). In other cases, the material has been dyed by an externally added chromophore (as in stained thin sections from a biopsy). In either case, it is often advantageous to be able to identify individual spectral components that are spatially collocated within the material, or to separate spatially the contributions from different spectral components within a complex image. An example of the former would be to resolve the overlapping absorption peaks of several photosynthetic pigments within a single chloroplast. An example of the latter would be to identify an eyespot within an algal cell based on its characteristic absorption spectrum, or to distinguish different species of algae within a complex population.

Macroscopic measurements. Up to now, obtaining accurate absorption spectra of microparticulate samples has relied on measurements using conventional methods, namely, macroscopic measurements in a spectrophotometer (see, e.g., Yentsch, 1962; Maske & Haardt, 1987) or microscopic measurements in a microspectrophotometer. Aside from the many well-documented optical problems that are associated with measuring pigmented particles in a spectrophotometer cuvette (such as light scattering (Bricaud *et al.*, 1983) and sieve effects (Duysens, 1956; Geider & Osborne, 1987)), there are also additional drawbacks in that: (a) the spectrum obtained from a bulk sample is only the statistical average of the individual micro-components (Sathyendranath *et al.*, 1987), and (b) microorganisms which cannot yet be cultured (Amann *et al.*, 1995) or solid matrices containing very "dilute" colored components simply cannot be assembled into a "bulk" sample for this type of analysis. In addition, the fact that the pigments are sometimes inhomogeneously distributed within each cell can affect the absorption measurement (Haardt & Maske, 1987). Although the pigments can often be extracted, the extraction procedure carries with it the risk of preparation artifacts, and it also cannot duplicate the original microenvironment of the chromophore. Accurate measurements of the *in vivo* absorption spectra of individual microorganisms could help to reduce the existing instrumental uncertainty in a broad range of

scientific studies. In marine biology, for example, it is known that errors in determining the absorption coefficients of phytoplankton can have a significant impact on estimates of population size and productivity in marine environments (Kishino *et al.*, 1985; Lewis *et al.*, 1985; Babin *et al.*, 1993). Dynamic environmental effects on subcellular structure and physiology, such as photoacclimation (Falkowski & LaRoche, 1991; Cunningham *et al.*, 1992), chromatic adaptation (Grossman *et al.*, 1993; Kehoe & Grossman, 1994), and nutrient deprivation (Chalup & Laws, 1990; Riess *et al.*, 1990) are also thought to be important for understanding the large-scale environmental biology of some algae and cyanobacteria, although their ecological significance is difficult to establish with currently available technology.

Microscopic measurements. Traditional microspectrophotometers (Zimmer, 1973; Thiessen & Thiessen, 1977; Chance, 1989,1991) overcome some of the drawbacks of macro-spectrophotometry because they can achieve the image magnification necessary to measure individual cells. However, the simplest of these (in which the spectrophotometer detector simply absorbs all of the light passing through the microscope objective) require the user to physically isolate the target cell(s) within the measuring beam in order to be assured of acquiring a correct spectrum (Strother & Wolken, 1959). Later adaptations of this design have incorporated opaque masks or measuring diaphragms to isolate a particular feature (Zimmer, 1973; Gualtieri *et al.*, 1989) or moving condensers to scan the image (Benedetti *et al.*, 1976). But in order to obtain and analyze distinct spectra from a large number of different components within an image (i.e., multiplexed acquisition), some kind of computerized image processing is essential. Several different types of "smart" microspectrophotometers have relied on a scanning Nipkow disc (Brugal *et al.*, 1979) or on a scanning stage (e.g., Thiessen & Thiessen, 1977; Ploem *et al.*, 1979; Zhang *et al.*, 1992; Seiyama *et al.*, 1994). These systems can only generate spectra from relatively limited parts of the image, or with limited spatial resolution. Early examples of scanned imaging microscopes have been reviewed by McMullan (1990).

New technologies for multi-spectral image processing. Despite these advances, it was nevertheless recognized that developing a massively parallel system to acquire and process full spectra from every pixel in a large image would require the combination of high-resolution detection and substantial computational power. In addition, algorithms to sort the spectra based on user-selected characteristics would be essential for comprehending such large datasets. One early instrument for acquiring radiometrically-calibrated spectra of macro-images was developed to screen pigmented colonies on Petri plates, and was termed the Filter Array Spectrophotometer or the Digital Imaging Spectrophotometer (Yang & Youvan, 1988; Arkin *et al.*, 1990). Digital imaging spectroscopy is defined as the combined analysis of both spatial and spectral information so that each picture element (pixel) in a two-dimensional scene includes a third dimension of spectral information. The original device used a set of Fabry-Perot interference filters to illuminate the sample at a series of wavelengths. The grayscale intensity of the transmitted light at each wavelength for each pixel was then converted to an absorbance value by a Silicon Graphics workstation. The spectrum of each pixel in the scene could then be calculated and displayed. The DIS instrument has been used to screen combinatorial libraries of mutants in the photosynthetic bacterium *Rhodobacter capsulatus* (Goldman & Youvan, 1992; Arkin & Youvan, 1993; Delagrave *et al.*, 1993; Delagrave & Youvan, 1993; Youvan, 1994; Youvan *et al.*, 1995; Delagrave *et al.*, 1995a) and to screen *E. coli* colonies expressing mutational variants of the green fluorescent protein (Delagrave *et al.*, 1995b). By employing this device, it is possible to simultaneously obtain radiometrically-calibrated absorption or fluorescence spectral information (between 400-950 nm) for up to 250,000 16-bit pixels simultaneously, as well as to sort the spectra by a number of different (user-defined) criteria. The original prototype imaging system

has been developed into a commercial instrument known as the *ColonyImager* (Youvan, 1994; Youvan *et al.*, 1995).

Rationale for HIRIM. HIRIM was designed to incorporate the principles of digital imaging spectroscopy embodied in the *ColonyImager* into a wide-field microscope system. With HIRIM and its software interface *CyberDIS*, scientists and engineers would be presented with a novel tool to obtain absorption spectra of microscopic samples. For example, rather than obtaining the average spectrum from a culture of microorganisms, HIRIM could be used to simultaneously acquire the spectra of hundreds of individual cells within the population. Likewise, HIRIM could also be used to acquire absorption spectra of subcellular features from other microscopic samples. This spectral information could then be sorted, categorized and correlated to morphological features captured in the image of the microscope's field of view. HIRIM also has a sister instrument, the Fluorescence Imaging Microspectrophotometer (FIMS), which is described in a companion paper (Youvan *et al.*, 1997).

Materials and Methods

Algal strains. In addition to samples supplied by scientists in the field, pure cultures of freshwater and marine organisms were obtained from the Provasoli-Guillard National Center for Culture of Marine Phytoplankton (CCMP) in West Boothbay Harbor, Maine. Organisms were selected based on a variety of characteristics, including pigment composition. For example, *Tetraselmis sp.*, *Rhodomonas salina*, *Skeletonema costatum* are natural and abundant food sources in coastal regions. These marine algae are also used as shellfish food in aquaculture. *Dunaliella tertiolecta* is a halophilic green algae cultivated in many countries for beta-carotene production. Many species of *Chrysochromulina* are toxic and known to be involved in red tide blooms, which have been devastating to the fish and shellfish industries (Moestrup, 1994). The coccolithophorid *Emiliana huxleyi* is a common bloom-forming alga in the open ocean which has been associated with bright areas in airborne and satellite images (Holligan *et al.*, 1983; Ackleson, 1990) of ocean waters. Such organisms play an important role in the global carbon cycle, since each cell is covered by numerous calcified scales known as coccoliths which are composed of almost pure calcium carbonate. Table 1 lists the taxonomic data, average cell size, and major pigments of some of the eukaryotic algae studied (only CCMP strains are listed). Although spectra were acquired for all of the species listed in Table 1, only a few representative examples will be described here.

Class	CCMP no.	Genus and Species	Size / μm	Major Pigments
-------	----------	-------------------	----------------------	----------------

Biotechnology et alia 4:1-20

Chlorophyceae	232	<i>Chlamydomonas</i> sp.	3-6 x 3-7	chl a,b; car, lut, vio, zea
	258	<i>Chlorococcum</i> sp.	4-12	
	259	<i>Chlorosarcinopsis halophilia</i>	12	
	1320	<i>Dunaliella tertiolecta</i>	6-9	
Prasinophyceae	903	<i>Tetraselmis</i> sp.	15-20 x 10-15	chl a,b,c; lut, zea
	1203	<i>Pycnococcus provasoli</i>	3	
Xanthophyceae	1275	<i>Tribonema aequale</i>	(filamentous)	chl a,c
Cryptophyceae	1168	<i>Chroomonas mesostigmatica</i>	3-7	chl a,c; AP, PC, PE, car
	1319	<i>Rhodomonas salina</i>	5-13 x 6-8	
Rhodophyceae	1328	<i>Porphoridium cruentum</i>	5-8	chl a,d; AP, PC, PE, car, lut
	1530	<i>Rhodorus</i> sp.	5-8	
Prymnesiophyceae	282	<i>Chrysochromulina ericina</i>	5-8	chl a,c; car, fux
	284	<i>Chrysochromulina herdensis</i>	5-8	
	373	<i>Emiliana huxleyi</i>	4-8	
	378	<i>Emiliana huxleyi</i>	4-8	
Chrysophyceae	678	<i>Poterioochromonas</i> sp.	4-7	chl a,c; car, fux, vio
Dinophyceae	685	<i>Prorocentrum lima</i>	45-48 x 30-33	chl a,c; fux
Coccinodiscophyceae	1315	<i>Chaetoceros calcitrans</i>	3-7	chl a,c; car, fux, vio
	1332	<i>Skeletonema costatum</i>	6-8	chl a,c; car, fux
Bacillariophyceae	1405	<i>Amphora</i> sp.	3-4 x 7-9	chl a,c; car, fux
Raphidophyceae	1596	<i>Heterosigma akashiwo</i>	9-12	chl a,c; car, fux, vio

Table 1. Genus and species, class, average cell dimensions, and major pigments of some of the algae examined by HIRIM. CCMP is the strain collection number assigned by the Provasoli-Guillard National Center for Culture of Marine Phytoplankton. The following pigment abbreviations apply: chl, chlorophyll; AP, allophycocyanin; PE, phycoerythrin; PC, phycocyanin; car, carotene; fux, fucoxanthin; lut, lutein; vio, violaxanthin; and zea, zeaxanthin.

Algal culture and sample preparation. Photosynthetic algae, like many land plants, may exhibit sensitivity to a photoperiodic cycle of day and night. Therefore, cultures were maintained in a temperature-controlled environment with periodic illumination. Algae were grown in Guillard's media (WC or f/2 obtained from Sigma) at 10 to 15°C at a light intensity of 40 $\mu\text{E m}^{-2} \text{s}^{-1}$. Cells were harvested in late exponential phase and concentrated by centrifugation in 1.5 ml aliquots at 4600 $\times g$ for 1 minute in a microcentrifuge. The supernatant was discarded and the pellet was resuspended in new media by gentle pipetting. The sample was then vortexed for 5 seconds and the supernatant again removed leaving behind a highly concentrated algal culture. In addition to concentration, these procedures helped to clear the sample of fine detritus and particulates which might interfere with subsequent spectral acquisition. Because care must be taken so that cells are not disrupted and filaments unduly severed, this procedure was modified depending on whether the organism is unicellular or filamentous. In some species, (e.g., *Fremyella diplosiphon*, *Amoebobacter purpureus*) individual organisms form filamentous masses or flocculants which must be dissociated to obtain meaningful spectra. In these cases, we experimented with gentle sonication and addition of detergents to separate these organisms. Other species are incapable of growing to a high density in liquid culture, and therefore they had to be concentrated by centrifugation in order to obtain sufficient cells to fill the microscope field.

Since Brownian motion and/or organism motility interferes with image registration during an instrument run, the algae first had to be immobilized on glass slides. However, many of the cells do not survive air drying and some cannot withstand heating. Therefore, cells must be embedded in an immobilizing matrix which is optically transparent and which does not adversely affect their morphology or their spectral properties. For these reasons, we chose to embed cells in 2 % (w/v) low-melt agarose (Reize & Melkonian, 1989) with 2 % NaCl added. To do this, an equal volume of cells and agarose-NaCl were mixed together on a glass microscope slide. (NaCl was omitted for freshwater samples.) The dissolved salt prevents the marine and/or halophilic organisms from lysing due to osmotic pressure differences. A coverslip was immediately placed over the mixture, and the cells were formed into a single layer by applying gentle pressure to the top surface of the coverslip, which was sealed by applying petroleum jelly to its edges. This method of sample preparation has enabled us to maintain reproducible spectra for up to 24 hours.

Tissue sections. Thin-sectioned cardiac tissue was stained with hematoxylin and eosin. The sample used in this study had been stained to identify potential amyloidosis, which is characteristic of certain types of cardiomyopathy (Olson *et al.*, 1987; Pepys, 1988). The sample was kindly provided by Prof. Philip Ursell of the University of California at San Francisco.

Spectra acquisition. Samples, prepared as described above, were initially examined under brightfield illumination along with preliminary focusing and alignment of the objects to be viewed within the selected field. The white light source was then replaced with a fiber optic coupled to a monochromator (Fig. 1). An image illuminated at a wavelength in the midrange for the intended scan was then acquired with the attached charged coupled device (CCD) camera and displayed on the computer screen. Many features of interest (typically, several hundred) can be selected from this image. One reference feature is also selected from the background in a clear area free from debris. This reference feature is analogous to the "blank" in a double beam, conventional spectrophotometer and its grayvalues are used as the I_0 value in the Beer-Lambert calculation. A preliminary calibration run was performed to correct for system response which would later be refined in real-time during the scan. Without further user interaction, *CyberDIS* software proceeds with the actual spectral scan, calculates spectra for all features, and then displays the results on the computer monitor in a form similar to that of Fig. 2.

Instrument Development

The CCD camera and driver. HIRIM incorporates a state-of-the-art, Peltier cooled CCD camera as its detector. This solid state linear photon counter exhibits very low noise as a result of efficient cooling. In addition, double correlated sampling is used in order to minimize readout noise. At 0 °C, the dark current in the KAIROS K7 camera is only 36 electrons per minute. For low-light applications requiring long integration times, light-minus-dark frame images can be readily acquired for increased sensitivity. Unlike many other commercial cameras which only digitize to 12 bits, the K7 can digitize to 16 bits, yielding a dynamic range of 0-65535 units of pixel grayvalue. Spatial resolution defined by the chip is 765 x 510 pixels. Alternatively, the K7 can be operated in a binned mode at one half this spatial resolution. Rapid data transfer to a personal computer (PC) is accomplished via a parallel interface so that a typical spectral scan from 430 to 730 nm in 5 nm increments can be acquired in minutes. A driver for

communications between the PC and the K7 camera was developed using low level C code that addresses the camera hardware directly. These functions were then incorporated into a Microsoft Windows program. Camera functions include: (1) establishment of communications protocols via the parallel port, (2) temperature control, (3) shutter control, (4) exposure time, and (5) data desampling and transfer options. The latter option enables the user to download either a complete image or a particular region of interest (ROI).

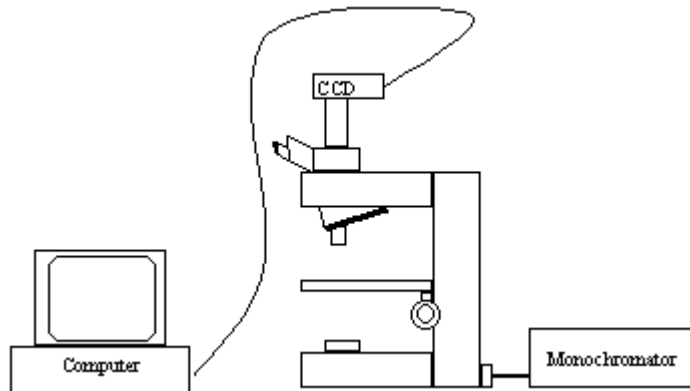


Fig. 1. Block diagram of the HIRIM instrument.

CCD and monochromator coupling to the microscope. The K7 camera has been coupled to the UTR-30 trinocular port of an Olympus BX60 microscope. This microscope features an on-axis vertical illumination system that facilitates both epifluorescence and brightfield microscopy. Rather than using customized relay lenses, we have designed and constructed a C-mount adapter for the trinocular port which achieves parfocality with the CCD chip and also accepts any standard camera lens. The output of an 1/8th m monochromator (1200 lines/nm, 350 nm blaze, Oriol) was directly coupled to the microscope via a fiber optic adapter which fit into the brightfield illuminator port. In order to optimize light throughput, the focal length of the first lens in the illumination system of the microscope was matched to the fiber optic bundle output as if it were held at a position in space corresponding to the normal QTH (quartz tungsten halogen) lamp.

Objective lenses. Microscope objective lens selection is an important concern when attempting to obtain radiometrically-calibrated spectra from essentially every pixel in an image. The quality of an objective is measured by its ability to correct chromatic and spherical aberrations. Chromatic aberration is due to the inability of the objective to focus light of different wavelengths at the same point. This has become an increasingly important consideration in the design and operation of spectral imaging microscopes, particularly in the confocal mode (see, e.g., Fricker & White, 1992). Spherical aberration is due to the inability to bring to focus at the same point the light that passes through the periphery of the lens and the light that passes through the center. An achromatic objective has been corrected at two wavelengths, (red and blue for chromatic aberration), and at a third wavelength in the yellow or green for spherical aberration. An apochromatic objective or apochromat is color-corrected at three wavelengths (red, yellow, and blue) and spherically corrected for two wavelengths. Objectives that contain fluorite, are also known as semi-apochromats. The quality of these objectives fall between an achromat and an apochromat. All of the objectives used in HIRIM

are infinity corrected and of the latter two categories; either apochromats or semi-apochromats. In addition to color corrected microscope objectives, HIRIM also incorporates an Olympus U-SC achromatic condenser.

Software and user interface. HIRIM instrument control, data display and analysis are all performed using *CyberDIS* software. Version 1.2 was written in C under the MS Windows 3.1 operating system. In addition to the camera communication functions described above, image processing, spectrum acquisition, spectrum analysis, and data export functions are also provided.

In a DIS type of application, the *CyberDIS* user interface consists of three windows: an image window, a conventional plot window, and a contour plot window (Fig. 2). The contour plot is a convenient visual tool to display three-dimensional data on a two dimensional surface, with a graded color scale representing the third dimension. The *x*-axis represents wavelength, the *y*-axis represents a particular feature (a set of contiguous pixels selected by the user), and the color scale represents a continuum of absorbance (where black/blue color represents no absorbance/small absorbance and red/white color represents high absorbance/maximum absorbance). The absorbance values are color-coded according to the color bar at the bottom of the contour window. Each row in the contour plot therefore corresponds to the spectrum of a given feature selected from the image. Pink/white areas correspond to peaks in the absorption spectrum for that feature. The *CyberDIS* user interface of HIRIM provides a convenient means to correlate features in the image with spectra, since the information is highlighted in all three windows simultaneously. Hence as Fig. 2 demonstrates, the computer mouse can be used to point to any feature in the image window or to any row in the contour map and generate a real-time update of the spectrum for that feature in the lower left window. Moving the red feature-selection circle across the image causes the small red bar at the left of the contour plot to move to the correct row; conversely, moving the red bar causes the corresponding feature to be marked in the image window, and its spectrum to be displayed in the spectrum plot window.

Results

Field sample analysis. The data shown in Fig. 2 were obtained from a field sample isolated from the surface waters of Stow Lake in Golden Gate Park (San Francisco, CA) during an algal bloom in March, 1995. Under a 40x objective, this image indicates the presence of a variety of cell types, including chlorophytes, diatoms and cyanobacteria. The highlighted feature is marked by a small red circle located in the lower left corner of the image. The spectrum of the organism under the circle is displayed in the lower left window as a conventional absorbance-versus-wavelength plot. In this dataset, 130 individual spectra from 430-730 nm were simultaneously acquired at 5 nm increments. As indicated by the presence of the scrollbar, only a fraction of these spectra are displayed in this view of the contour plot. The sorting algorithm is able to segregate a number of different spectral types, while simultaneously separating pigmented features away from debris.

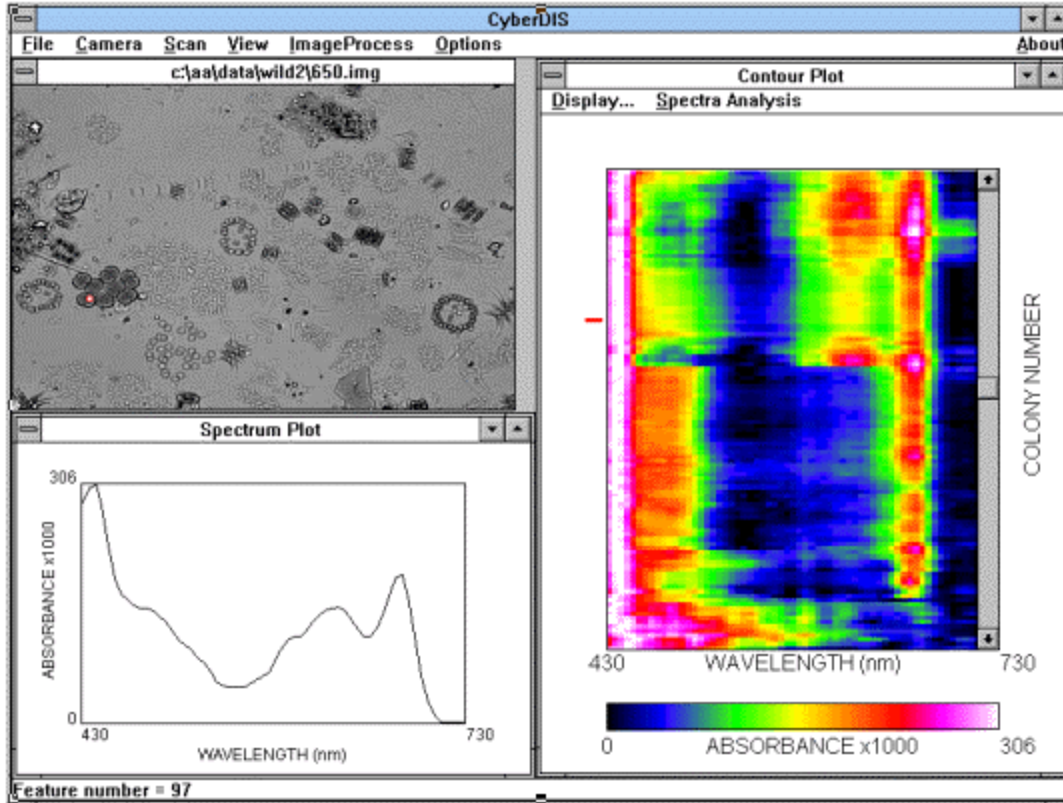


Fig. 2. *CyberDIS* user interface showing data acquired from a field sample collected during a green algal bloom. The text describes the interactions among the three windows.

Sorting of large datasets. One of the unique features of the software interface for HIRIM is its ability to sort spectra and display them in the form of pseudocolored contour plots. Sorting is important for reducing the effort needed to interpret spectral data from complex images. The versatility and power of these sorting functions are demonstrated using cultures of *Rhodospirillum rubrum*, *Chroomonas*, and *Chlorococcum*, which were mixed together and immobilized on a single slide (Fig. 3). Visual identification and sorting of these three algal types can be difficult, since all three are coccoid in shape and their sizes overlap in the range of 4-12 μm . Within the field of view for the image shown in Fig. 3 there were many intact cells, but there was also debris from the medium and debris from fragments of cells which had lysed. No *a priori* choice was made regarding which features were to be selected for analysis (i.e., both debris and intact cells were scanned). All 75 feature spectra are shown in each of the four panels in Fig. 3.

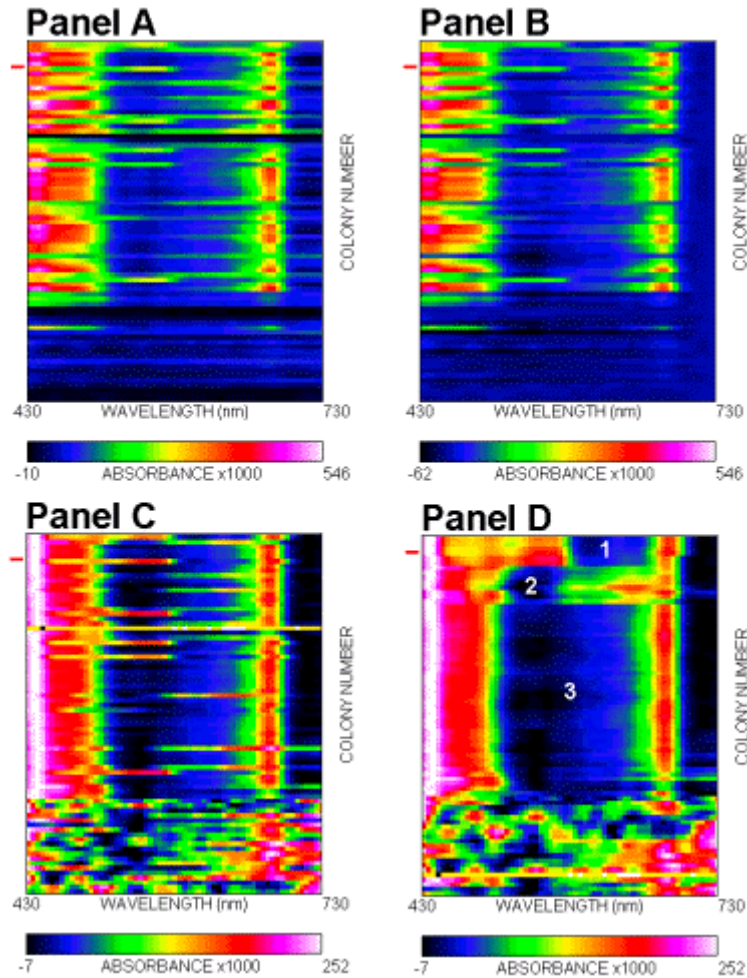


Fig. 3. Sequentially processed color contour maps of 75 spectral features from a sample containing three different algal types (see text).

The sorting paradigm used in Fig. 3 effectively sorts algae and debris. This procedure begins with the unprocessed contour map as it is displayed immediately after the scan (Panel A). Next, a constant value was subtracted to reset the baseline in each individual spectrum so that the absorbance at 730 nm is zero (Panel B). This adjustment is reflected as a consistent vertical dark stripe at the extreme right edge of the contour plot. Large absorption peaks due to chlorophyll (at approximately 430 nm and 680 nm), as well as from other pigments, can be seen as white/red areas in each row of the plot. Panel C shows the result of stretching each spectrum (i.e., each row) to its own minimum and maximum absorbance. This is in contrast to the pseudocoloring scheme in Panels A and B, where the absorbance values of each feature were scaled to the highest and lowest values obtained from the *entire* dataset. In Panel D, a least-squares algorithm has been applied so that similar spectra are grouped together. As Panel D shows, three spectral groupings are generated by applying this sorting algorithm, and the resultant spectral types reflect the three species which are present. Sorted contour plots can be used to visualize a number of useful experimental parameters. For example, the number of features contained in each spectral grouping could potentially be used to estimate the relative numbers of each species in the overall population. It is also important to note that this sorting procedure automatically places all aberrant spectra (arising from debris and other unidentifiable objects) toward the bottom of the contour map. In addition to similarity-sorting,

spectra can be sorted based on overall maximum absorbance, wavelength of maximum absorbance, and maximum absorbance at a particular wavelength. The ability to display color-coded first derivative contour plots has also been included in the analysis software. This option should be useful for analyzing subtle spectral features, such as the point of maximum slope between 680 and 740 nm, known as the “red-edge” effect. This feature has been widely studied in canopy and remote sensing and is believed to be related to chlorophyll and other pigments concentrations, leaf area index, and nutrient deficiencies (Curran *et al.*, 1991; Danson & Plummer, 1995; Boyer *et al.*, 1988).

A survey of absorption spectra from single cells. The organisms analyzed in the previous figure are from the classes *Chlorophyceae*, *Cryptophyceae*, and *Rhodophyceae*. In Fig. 4 we show representative spectra of eight different species representing 7 different classes, as measured by HIRIM on individual cells. The chlorophyll *a* peak at 675 nm is apparent in all 8 spectra. Chlorophyll *b* is found in *Dunaliella* and *Tetraselmis* (Traces G, & H). Its spectrum has a strong transition at 480 nm and a weaker transition at 650 nm. The latter is often seen as an asymmetric contribution to the stronger chlorophyll *a* peak at 675 nm. Phycobiliproteins are found in the *Cryptophyceae* and *Rhodophyceae* and are predominantly responsible for absorption between 450 and 650 nm. Carotene and xanthophyll pigments generally absorb at higher energies and exhibit extensive spectral overlap in this region.

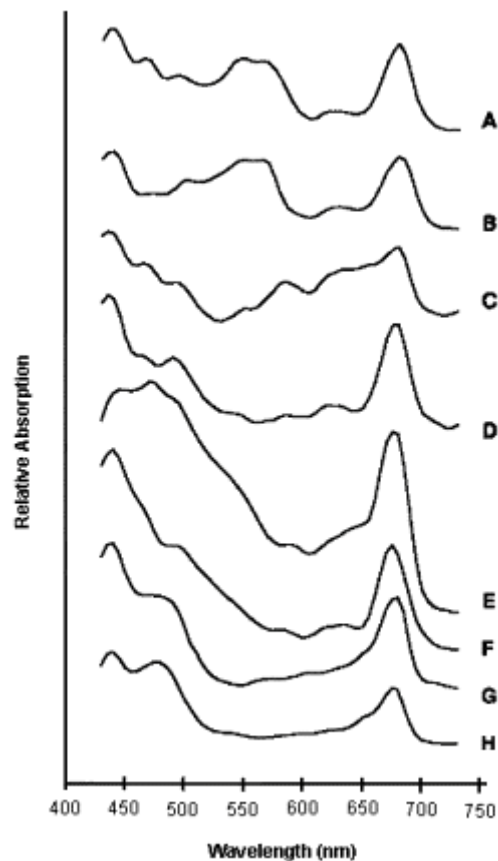


Fig. 4. HIRIM single cell spectra of: A) *Rhodomonas salina*, B) *Porphyridium cruentum*, C) *Chroomonas mesostigmatica*, D) *Tribonema aequale*, E) *Prorocentrum lima*, F) *Amphora sp.*, G) *Dunaliella tertiolecta*, and H) *Tetraselmis sp.*

All of the HIRIM spectra shown in Fig. 4 correlate well with published spectra of extracted pigments or cell cultures taken on a conventional spectrophotometer with a scattering

attachment (see Häder & Tevini, 1987; Rowan, 1989). Due to the wide variation in cell size, HIRIM spectra were acquired over a full range of magnifications: 10×, 20×, 40× air-based semi-apochromat, and the 100× oil immersion apochromat objectives were used.

Spectra from subcellular structures: HIRIM lends itself to the spectral analysis of subcellular structures. Out of the list of organisms in Table 1, we have performed preliminary studies of eyespot granules in *Chlamydomonas* and *Tetraselmis*. In both cases, broad, enhanced absorption in the blue was measured when the feature selection circle was placed over an eyespot. (This result is in contrast with the observation of two peaks at 440 and 485 nm when the feature selection circles are placed over chloroplasts.) For *Chlamydomonas*, these spectra are consistent with the presence of the carotenoid-rich globules that constitute the eyespot apparatus (Grung *et al.*, 1994), along with a possible contribution from the retinal-based photoreceptor pigment in the vicinity of the eyespot (Beckmann & Hegemann, 1991).

Here we demonstrate HIRIM's ability to obtain subcellular spectra using a single cell of *Gymnodinium fuscum* during a pre-germination stage of its life cycle. In this form, *Gymnodinium* undergoes a maturation process wherein plastids are bleached, starch granules become indistinct, and masses of red oil begin to appear (Lee, 1992). The reference image in Fig. 5 has been pseudocolored by combining the contrast enhanced images taken at 450, 550, and 650 nm and coding their respective grayvalues as intensities for the red, green, and blue color guns in the phosphor screen display of the computer monitor. This process enhances the location of the red oil masses for better visualizations while generating a green background. The full-scale contour plot shows 70 spectra corresponding to 70 randomly selected features placed on the image of the cell. One of these features is highlighted as a filled white circle on the image, and its absorption spectrum is shown in the spectrum plot window. The contour plot has been sorted based on the maximum absorption at 520 nm. As evidenced by the trend from white to pink to green, features with the highest absorbances at this wavelength are grouped towards the bottom and represent reddish brown areas in the image. Looking at chlorophyll absorption represented by the vertical column located at 670 nm, it is important to note how rapidly one can detect the absence of spectral shifts using *CyberDIS* software. If one were to view this same contour plot in a full-scale mode, the highest absorbance of each feature spectrum (row) would be encoded as white. The information obtained in this display mode would also facilitate the identification of oil-free areas, since all these features would line up and show a peak maximum (white) at 460 nm as opposed to 520 nm.

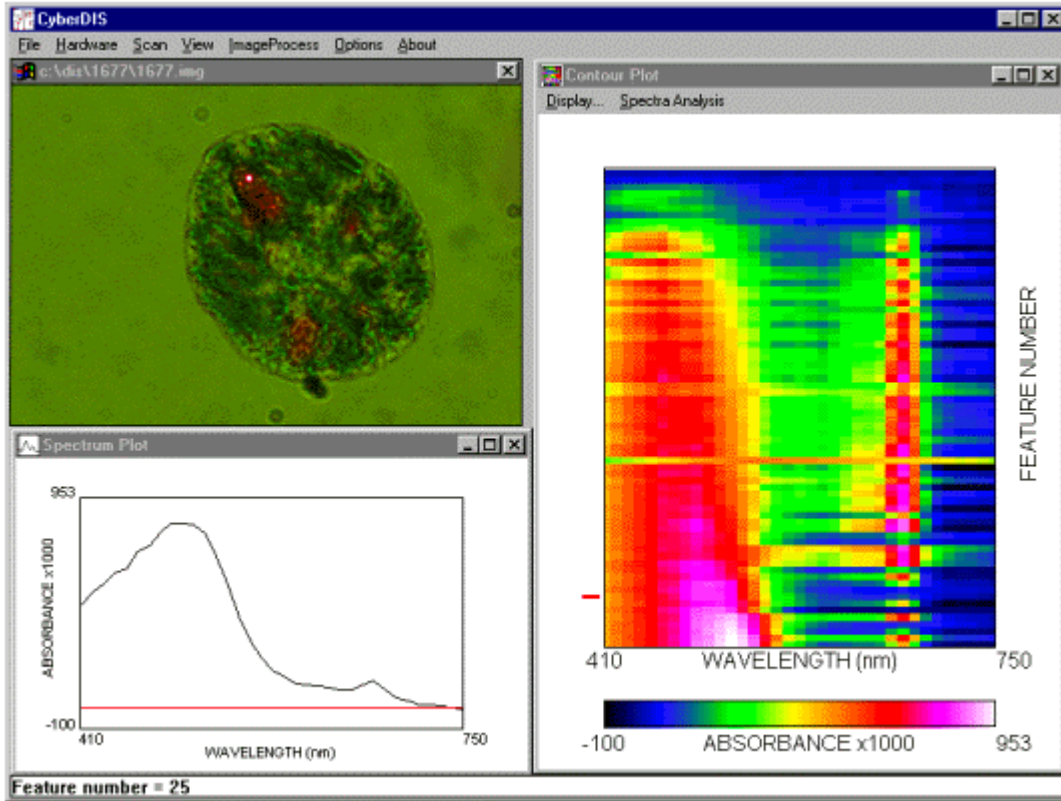


Fig. 5. HIRIM image of a *Gymnodinium* cell and subcellular absorption spectra.

HIRIM analysis of H&E stained tissue sections. In order to test the versatility of HIRIM for cell biology applications, we analyzed a typical slide from a histopathology laboratory. This slide (Fig. 6) holds a thin section of biopsied cardiac tissue stained with hematoxylin and eosin. H&E treatment is used to stain cell nuclei, basophilic cytoplasmic structures, some elastic fibers and mucins with a blue-purple color, while most of the other structures are stained shades of red. Fig. 6 shows the results of a scan of this tissue. The spectral window at the lower left shows the spectrum obtained from an area of tissue marked by the circle in the image window. In the image, the circle is located in an area of the tissue where one would expect only the eosin counterstain to bind; and indeed, the spectrum of this feature (a peak at 535 nm with a shoulder on the short-wavelength side), is virtually identical to that of eosin in solution (Green, 1991). Features which segregate to the bottom show spectral characteristics of both H&E dyes.

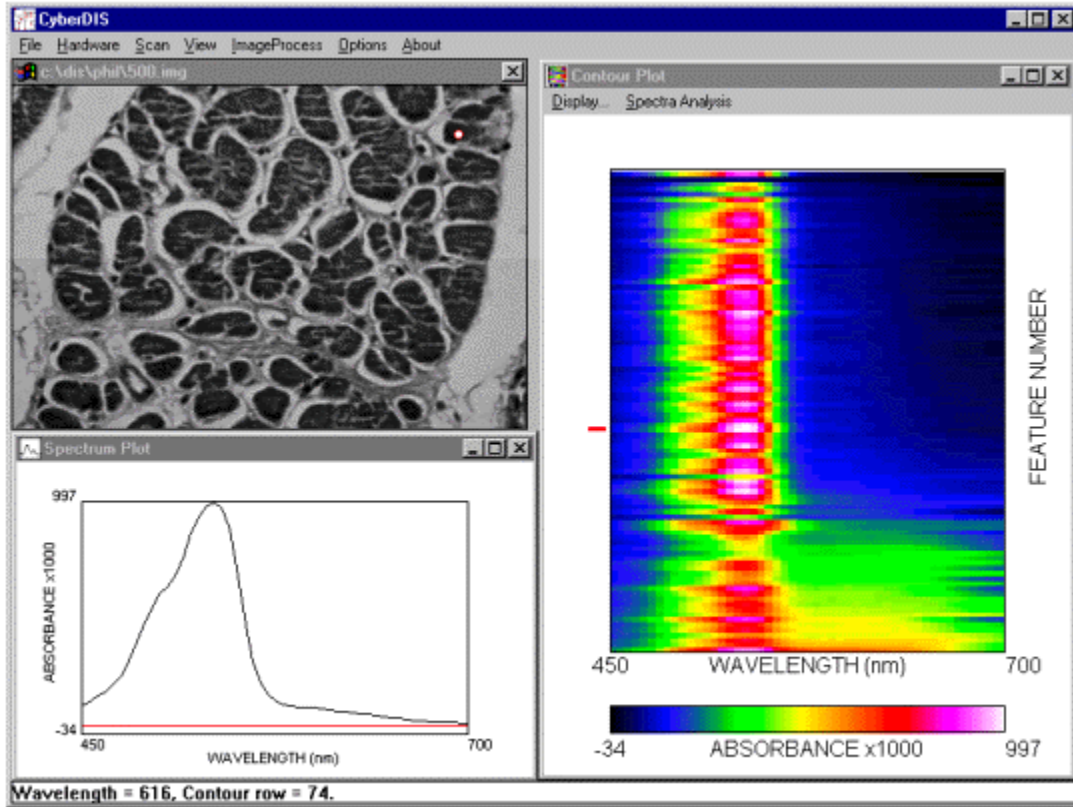


Fig. 6. HIRIM spectra of a thin section of biopsied cardiac tissue stained with hematoxylin and eosin.

In order to be used as a stain, hematoxylin is oxidized to hematein which then forms metal chelates which range in color from red-violet to blue-black, depending on the metal chelated. In many cases, a further oxidized product, oxyhematein (brown), is irreversibly formed (Prento & Shulte, 1991). This complex chemistry often results in a very broad peak similar to that found in cell nuclei spectra in our tissue sample. A conventional plot with representative spectra of such features is not shown. However, it can be seen from the contour plot that tissue spectra (94 total) sort into two distinct spectral categories based on absorption at 620 nm.

Discussion

Studies of marine and freshwater algae. Haardt & Maske (1987) have discussed the premise that determining the light absorption characteristics of phytoplankton is essential to understanding primary production in the sea. To test this idea, they took absorption spectra of marine algae and made corrections for both the presence of detritus in the samples and the high background absorbance of water and dissolved matter. These corrections can be made easily with the HIRIM system described here, since features can be selected from individual cells and, if desired, from the detrital particles. For the individual cells themselves, no correction for interference by detrital particulate matter in the sample is necessary. With the HIRIM system, absorption spectra of cells in unprocessed field samples can be taken independently of other sample components, so that the spectra of rare species can be

extracted without being masked by the dominant species. In the Stow Lake image, for example, the dominating algae were chlorophytes, and yet spectra from diatoms could be identified, which, in a bulk measurement, would have been completely masked (see Fig. 2). Combined spectra related to the relative abundance of each type of alga in the sample can be compared to spectra taken of the whole sample by more conventional methods. These data can, in turn, be compared with those obtained through remote sensing in order to estimate how well the average absorption spectra correspond to remote measurements of the composition of alga types in lakes and oceans. Additional studies of the effects of nutrient stress and changes in illumination conditions on the *in vivo* spectra of pigments might also be informative.

In terms of spectral identification of pigments, the HIRIM instrument can identify pigments localized in subcellular organelles, a task which is virtually impossible to do in a conventional spectrophotometer without first isolating the organelle and (because of scattering and sieve-effect problems) extracting the pigment. The risk of preparation artifacts is therefore significant (Haardt & Maske, 1987). And although micro-spectrophotometers have been used previously to examine such organelles *in vivo* (Strother & Wolken, 1960; Gualtieri *et al.*, 1989), the ability of other microscope-based instruments to analyze complex images containing large numbers of cells is generally limited. This is particularly apparent for highly heterogeneous populations of cells, where the ability of the HIRIM sorting algorithms to organize numerous sub-populations of features and spectra into meaningful groups greatly accelerates data analysis and interpretation. This capability might be advantageous for comparing different pigmentation mutants. Finally, from an analytical chemistry perspective, it is noteworthy that sieve or packaging effects on the absorption spectra are also minimized in the HIRIM system due to the extremely short optical pathlength. This characteristic is important for determining correct *in vivo* absorbances at peak absorption wavelengths in optically dense pigmented cells.

Studies of stained tissues and cells. Despite the power of more recently developed techniques such as electron microscopy, fluorescence microscopy, and atomic force microscopy in the analysis of biological materials, the brightfield microscope still remains the primary tool of pathologists in the initial survey of biopsied tissue. We chose here, as an example from the health sciences field, to analyze an H & E stained tissue sample, but the discussion and concepts are clearly applicable to many other types of staining procedures in histochemistry and diagnostic microbiology.

Compared to the human eye, HIRIM has the ability to measure hundreds of spectral bands with a resolution of 2 nm. The human eye however, relies on only three spectral bands: blue, green, and red. These in turn correspond to the three visual pigments (i.e. rhodopsins) (Marr, 1982), which have very broad and overlapping absorption through the visible spectrum. Human color perception is easily fooled by metameric colors. For example, pink can be generated by a mixture of white light and an orange hue, or a mixture of red and cyan, or a mixture of violet, green and red. Each of these combinations has a spectroscopic signature not detected by the eye. The absorption spectra of features in stained sections may contain inherent information which is not currently perceived by pathologists. It should be noted that many of the staining procedures are not standardized because the staining process is difficult to control. Subtle color differences are often described as “pinkish” or “orangish” or “with a yellow tinge”. When color description is ambiguous, it would be beneficial to have full spectral information. This additional knowledge may be sufficient to resolve cases where a specimen would have previously required a second (or multiple) more expensive stain which would need to be applied to a different tissue section. Our first study of cardiac tissue was conducted to determine whether spectral differences in peak shape or position existed between amyloid and

other connective tissue, both of which stain various shades of pink with H&E. This is a case where morphological differences may be inadequate to differentiate amyloid, which is characteristic of certain types of cardiomyopathy, from normal tissue. Our preliminary results are promising, and it appears that the potential for using HIRIM in similar applications is essentially untapped.

Evaluation of HIRIM capabilities. HIRIM was designed to be a useful instrument for massively parallel acquisition and analysis of absorption spectra from microscopic samples. We have attempted to demonstrate its capabilities by obtaining high resolution spectra of such diverse biological targets as highly pigmented marine and freshwater microorganisms and stained tissue sections. The ability to perform these measurements on complex samples may have implications for a number of other types of scientific measurements and surveys. In the area of remote sensing and environmental monitoring, for example, HIRIM could potentially provide a database of individual spectra for well-defined microbial samples, which could then be compiled and correlated with the spectra of various pigments in each cell. This database could then be used to validate satellite-based measurements of algal blooms and phytoplankton population dynamics. Similarly, it could be used in quantitative cell biology and medicine to standardize staining and tissue preparation procedures, and to correlate the results of testing based on key spectral features and absorbance values. In the study of microbial diversity (Hugenholtz & Pace, 1994; Giovannoni *et al.*, 1996) and taxonomic composition (Andersen *et al.*, 1996) HIRIM could be used to complement existing technology. The combination of novel hardware and software incorporated into HIRIM has been designed to overcome many of the spectroscopic and image processing limitations found in earlier instruments. Nevertheless, several challenges remain. Although the quality of the spectra shown here is representative of the data acquired, in a few instances we have noted the appearance of noise, sudden changes in slope, and other features which necessitate further investigation. These artifacts are more problematic as one approaches the diffraction limitation of light microscopy ($\sim 1 \mu\text{m}$; Inoué, 1989). In some cases, spherical cells may act as a crude lens by either dispersing or concentrating the brightfield light. If the cell has a higher index of refraction than the embedding medium, it will act as a converging lens and concentrate light within the cell image. These problems are particularly evident in organisms with calcium carbonate or silica shells. In these cases, different embedding media may need to be employed, and it may also be necessary to restrict the spectral calculations to pixels from features which lie well within cell walls and away from areas where sudden changes in the index of refraction occur. These feature-selection guidelines also apply to membranes, plastids, and the nuclei within the cell infrastructure. We are continuing to investigate this phenomenon and its effect on the spectra as we attempt to analyze single cells or small features in the 1-2 μm size range. Correlation between a morphological feature identified by HIRIM and morphological information obtained from other techniques, such as electron microscopy, can also be used to confirm the validity of a particular observation.

Biotechnology. In addition to the biological aspects discussed above, there are a number of potential avenues open for applying multi-spectral imaging to biotechnology. These include both naturally pigmented cells and materials as well as material stained by exogenous dyes or chromogens. Among the areas that might benefit from this technology are: (1) metabolic engineering using chromogenic substrates, (2) analysis of microbial diversity, (3) identification of natural products, (4) screening for novel biosynthetic dyes and pigments, (5) hemoglobin analysis, (6) development of antibiotics, (7) screening of drug effects on cell metabolism and development, (8) air and water quality testing and (9) bioremediation.

Materials science and quality control. Further development of HIRIM technology will undoubtedly include areas outside of biology, medicine and biotechnology. HIRIM could easily be adapted to analyze materials such as mineral thin sections for mineralogy, gemology, and civil engineering. It could also be employed in the study of materials processing and quality control for both natural and synthetic materials (paper, textiles, ceramics, polymers, optically-transparent materials, thin films, optical coatings, semiconductor materials, etc.). Microscopic defects and anomalies having characteristic spectral “fingerprints” can be identified and sorted without the burden of excessive sample preparation and manual data analysis.

Acknowledgments

We would like to thank Harriet Jones for technical assistance, Philip Ursell (UCSF) for kindly providing cardiac tissue samples, Robert A. Andersen (CCMP) for helpful discussions regarding phytoplankton pigment compositions, and Reinhard Enders (Olympus) for technical advice on brightfield microscopes. This work has been supported by NAS2-14386. HIRIM is patent pending.

References

- Ackleson, G. (1990) *EOS* **71**:108.
- Amann, R.I., Ludwig, W. & Schleifer, K.-H. (1995) *Microbiol. Rev.* **59**:143-169.
- Andersen, R.A., Bidigare, R.R., Keller, M.D., and Latasa, M. (1996) *Deep-Sea Research II, Topical Studies in Oceanography*, **43**:517-537.
- Arkin, A.P., Goldman, E.R., Robles, S.J., Goddard, C.A., Coleman, W.J., Yang, M.M. & Youvan, D.C. (1990) *Bio/Technology* **8**:746-749.
- Arkin, A.P. & Youvan, D.C. (1993) In: *The Photosynthetic Reaction Center, Vol. I* (Deisenhofer, J. & Norris, J.R., eds.) pp. 133-155, Academic Press, New York.
- Babin, M., Therriault, J.-C., Legendre, L. & Condal, A. (1993) *Limnol. Oceanogr.* **38**:154-177.
- Beckmann, M. & Hegemann, P. (1991) *Biochemistry* **30**:3692-3697.
- Benedetti, P.A., Bianchini, G., & Chiti, G. (1976) *Appl. Opt.* **15**:2554-2558.
- Boyer, M., Miller, J., Belanger, M. & Hare, E. (1988) *Remote Sens. Environ.* **25**:71-87.
- Bricaud, A.A., Morel, A. & Prieur, L. (1983) *Limnol. Oceanogr.* **28**:816-832.
- Brugal, G., Garbay, C., Giroud, F., & Adelh, D. (1979) *J. Histochem. Cytochem.* **27**:144-152.
- Chalup, M.S. & Laws, E.A. (1990) *Limnol. Oceanogr.* **35**:583-596.
- Chance, B. (1989) In: *Cell Structure and Function by Microspectrofluorometry* (Kohen, E. & Hirschberg, J.G., eds.) pp. 53-69, Academic Press, San Diego.

- Chance, B. (1991) *Annu. Rev. Biophys. Biophys. Chem.* **20**:1-28.
- Cunningham, F.X., Vonshak, A. & Gantt, E. (1992) *Plant Physiol.* **100**:1142-1149.
- Curran, P.J., Dungan, J.L., Macler, B.A. & Plummer, S.E. (1991) *Remote Sens. Environ.* **35**:69-76.
- Danson, F.M. & Plummer, S.E. (1995) *Intl. J. Remote Sens.* **16**:183-188.
- Delagrave, S. & Youvan, D.C. (1993) *Bio/Technology* **11**:1548-1552.
- Delagrave, S., Goldman, E.R. & Youvan, D.C. (1993) *Prot. Eng.* **6**:327-331.
- Delagrave, S., Goldman, E.R. & Youvan, D.C. (1995a) *Prot. Eng.* **8**:237-242.
- Delagrave, S., Hawtin, R.E., Silva, C.M., Yang, M.M. & Youvan, D.C. (1995b) *Biotechnology* **13**:151-154.
- Duysens, L.N.M. (1956) *Biochim. Biophys. Acta* **19**:1-12.
- Falkowski, P.G. & LaRoche, J. (1991) *J. Phycol.* **27**:8-14.
- Fricker, M.D. & White, N.S. (1992) *J. Microsc.* **166**:29-42.
- Geider, R.J. & Osborne, B.A. (1987) *Marine Biol.* **96**:299-308.
- Giovannoni, S.J., Rappé, M.S., Gordon, D., Urbach, E., Suzuki, M., & Field, K.G. (1996). In: *Evolution of Microbial Life* (Roberts, D.M., Sharp, P., Alderson, G., & Collins, M., eds.) pp. 63-85, Cambridge Univ. Press, New York.
- Goldman, E.R. & Youvan, D.C. (1992) *Bio/Technology* **10**:1557-1561.
- Green, F.J. (1991) *The Sigma-Aldrich Handbook of Stains, Dyes and Indicators*, Aldrich Chemical Company, Milwaukee.
- Grossman, A.R., Schaefer, M.R., Chiang, G.G. & Collier, J.L. (1993) *Microbiol. Rev.* **57**:725-749.
- Grung, M., Kreimer, G., Calenberg, M., Melkonian, M. & Liaaen-Jensen, S. (1994) *Planta* **193**:38-43.
- Gualtieri, P., Passarelli, V. & Barsanti, L. (1989) *Micron Microsc. Acta* **20**:107-110.
- Haardt, H. & Maske, H. (1987) *Limnol. Oceanogr.* **32**:608-619.
- Häder, D. & Tevini, M. (1987) *General Photobiology*, Pergamon Press, Oxford.

- Holligan, P., Voillier, M., Harbour, D.S., Camus, P. & Champagne-Phillippe, M. (1983) *Nature* **304**:339-342.
- Hugenholtz, P., & Pace, N. (1996) *Trends Biotechnol.* **14**:190-197.
- Inoué, S. (1989) *Methods Cell Biol.* **30**:85-112.
- Kehoe, D.M. & Grossman, A.R. (1994) *Seminars Cell Biol.* **5**:303-313.
- Kishino, M., Takahashi, M., Okami, N. & Ichimura, S. (1985) *Bull. Marine Sci.* **37**:634-642.
- Lee, R.E. (1992) *Phycology*, Cambridge University Press, Cambridge.
- Lewis, M.R., Warnock, R.E. & Platt, T. (1985) *Limnol. Oceanogr.* **30**:794-806.
- Marr, D. (1982) *Vision*, W.H. Freeman and Co., New York.
- Maske, H. and Haardt, H. (1987) *Limnol. Oceanogr.* **32**:620-633.
- McMullen, D., (1990) *Proc. Royal Microsc. Soc.* **25**:127-131.
- Moestrup, O. (1994) In: *The Haptophyte Algae* (Green, J.C. & Leadbeater, B.S., eds.) pp. 265-285, Clarendon Press, Oxford.
- Olson, L. J., Gertz, M.A., Edwards, W.D., Li, C-Y, Pellikka, P.A., Holmes Jr., D.R., Tajik, A.J. & Kyle, R.A. (1987) *New England J. Med.* **317**:738-742.
- Pepys, M.B. (1988) *Quart. J. Med.* **67**: 283-298.
- Ploem, J.S., Verwoerd, N., Bonnet, J. & Koper, G. (1979) *J. Histochem. Cytochem.* **27**:136-143.
- Prento, P. & Schulte, E. (1991) In: *Theory and Strategy in Histochemistry* (Lyon, H., ed.) pp. 107-119, Springer Verlag, Berlin.
- Reize, I.B. & Melkonian, M. (1989) *Bot. Acta* **102**:145-151.
- Riess, M.H., Damm, I. & Grimme, L.H. (1990) In: *Current Research in Photosynthesis, Vol. IV* (Baltscheffsky, M., ed.) pp. 405-408, Kluwer Academic Publishers, Dordrecht, The Netherlands.
- Rowan, K.S. (1989) *Photosynthetic Pigments of Algae*, Cambridge University Press, New York.
- Sathyendranath, S., Lazzara, L. & Prieur, L. (1987) *Limnol. Oceanogr.* **32**:403-415.
- Seiyama, A., Chen, S.-S., Kosaka, H., & Shiga, T. (1994) *J. Microsc.* **175**:84-89.
- Strother, G.K. & Wolken, J.J. (1959) *Science* **130**:1084-1088.
- Strother, G.K. & Wolken, J.J. (1960) *Nature* **188**:601-602.

Thiessen, G. & Thiessen, H. (1977) *Progr. Histochem. Cytochem.* **9**:1-156.

Yang, M. M. & Youvan, D. C. (1988) *Bio/Technology* **6**:939-942.

Yentsch, C.S. (1962) *Limnol. Oceanogr.* **7**:207-217.

Youvan, D.C. (1994) *Nature* **369**:79-80.

Youvan, D.C., Goldman, E.R., Delagrave, S. & Yang, M.M. (1995) *Methods Enzymol.* **246**:732-748.

Youvan, D.C., Coleman, J.C., Silva, C.M., Petersen, J., Bylina, E.J., & Yang, M.M. (1997) *Biotechnology et alia*, <www.et-al.com>**1**:1-16.

Zimmer, H. G. (1973) In: *Micromethods in Molecular Biology* (Neuhoff, V., ed.) pp. 297- 328, Springer-Verlag, Berlin.

Zhang, C.Z., Young, W.G. & Basford, K.E. (1992) *J. Microsc.* **167**:233-237.